Available online at www.sciencedirect.com
SCIENCE DIRECT
Polymer 46 (2005) 785–798
polymer
www.elsevier.com/locate/polymer

The influence of cure conditions on the morphology and phase distribution in a rubber-modified epoxy resin using scanning electron microscopy and atomic force microscopy ☆

Bobby Russell[a], Richard Chartoff[b,*]

[a]BWXT Pantex, LLC, P.O. Box 30020, Amarillo, TX 79120, USA
[b]Department of Materials Science and Engineering, University of Arizona, 4715 E Fort Lowell Road, Tucson, AZ 85712, USA

Received 4 August 2004; received in revised form 15 November 2004; accepted 16 November 2004
Available online 13 December 2004

Abstract

In this paper, we consider the effect of cure conditions on the morphology and distribution of the rubber in a phase separated rubber-modified epoxy resin, which in effect is a two phase composite. Novel aspects of this study were measuring the elastic modulus of the dispersed rubber phase particles by atomic force microscopy (AFM) and verifying the presence of nano-dispersed rubber.

The purpose of introducing dispersed rubber particles into the primary phase in these systems is to enhance their toughness. It is known that both the rubber particle size and volume fraction affect the degree to which the epoxy is toughened. It is not known, however, how the specific mechanical properties of the rubber phase itself affect the toughness.

The objectives of this study were to: (1) use scanning electron microscopy (SEM) and atomic force microscopy (AFM) to determine the morphology and phase distribution of the rubber particles and (2) to measure the mechanical properties of the rubber particles using AFM. Ultimately, we would like to develop a clear understanding of how the changes in morphology and mechanical properties measured at the micro and nano-scales affect both the elastic modulus and fracture toughness of rubber-modified epoxy polymers.

The epoxy system consisted of a diglycidyl ether of bisphenol-A, Epon 828, cured with piperidine and incorporating a liquid carboxyl-terminated acrlonitrile-butadiene rubber (CTBN). The carboxyl groups of the rubber are capable of reacting with the epoxy. The cure conditions considered were based on a statistically designed full factorial curing matrix, with the variables selected being cure temperature, initiator (piperidine) concentration, and rubber acrylonitrile concentration.

Each of these primary variables was found to affect the phase distribution that resulted during cure. A statistical analysis of the effect of these variables on the phase morphology showed that the acrylonitrile content (%) of the rubber affected both the rubber particle size and volume fraction. The cure temperature strongly influenced the rubber particle volume fraction and modulus. Volume fractions of the rubber phase of up to 24% were obtained even though the amount of rubber added was only 12.5%. The rubber particle modulus varied from 6.20 to 7.16 MPa. Both the volume fraction and modulus of the rubber particles were found to influence the macroscopic mechanical properties of the composite. While larger volume fractions favor improved toughness, we note that that the toughness is greatest when the particle modulus values do not exceed ~6.2 MPa. Thus, increased volume fraction by itself may not always result in increased toughness. The particles also must be sufficiently 'soft' in order to improve toughness. In the system of interest here, the processing conditions are a key factor in achieving the most appropriate material properties. By inference, this is likely to be the case as well in other rubber-modified thermosets.

Keywords: Rubber-modified epoxy; Phase distribution; Toughened thermoset

1. Introduction

Epoxy resins are thermoset polymers that exhibit good adhesion; high strength; resistance to creep, heat, and chemicals; and they exhibit low cure shrinkage [1–3].

☆This research was carried out at the University of Dayton.

* Corresponding author. Tel.: +1 520 322 2979; fax: +1 520 322 2993.
E-mail address: chartoff@mse.arizona.edu (R. Chartoff).

0032-3861/$ - see front matter © 2004 Elsevier Ltd. All rights reserved.
doi:10.1016/j.polymer.2004.11.090

Conversely, these polymers are brittle as well as sensitive to moisture, and they exhibit poor toughness [3,4]. Their toughness is often improved by introducing a dispersed rubber phase into the primary epoxy phase [2–14]. The rubber is introduced prior to polymerization as a miscible liquid mixed into the uncured epoxy. The molecular weight of the liquid rubber is around 3000 and it contains functional groups that can react with and bond covalently to the epoxy phase. In this study, the rubber is a carboxyl terminated acrylonitrile-butadienne copolymer (CTBN).

During the polymerization, the rubber phase separates because it becomes less miscible with the matrix, forming tiny particles of rubber that are dispersed in the matrix [8, 15]. The diameters of the rubber particles are typically between 0.5 and 5 μm [11], and their volume fraction ranges between 5 and 30% [14]. The physical nature of the rubber particles may differ depending on the CTBN composition and the cure time and temperature. The rubber particles may be fairly homogeneous or heterogeneous, containing an occluded epoxy phase as indicated in the 'morphology' diagram of Fig. 1. Thus the 'rubber' phase is more precisely a rubber-rich phase, but for convenience in this paper we refer to it simply as the rubber phase. Similarly, the epoxy phase is an epoxy-rich phase that retains some rubber. At low rubber concentrations, the presence of a dispersed, secondary rubber phase can improve the fracture toughness without significantly diminishing the polymer's other properties such as elastic modulus and glass transition temperature [1,16,17]. Thus the fracture toughness of rubber-modified epoxies is often greater than for unmodified epoxies [4,8,9,12].

It is known that the morphology of the cured system, particularly the particle size [5–7,9,12,13] and volume fraction of the rubber phase [6,7,9,14–18], affect the degree to which the epoxy is toughened. The volume fraction is most important. Increased particle volume fractions often lead to improved toughness. Thus the occluded phase particle morphology is usually cited as 'preferred' because it results in larger particle volume fractions. It is not known, however, how the specific mechanical properties of the rubber phase affect the toughness.

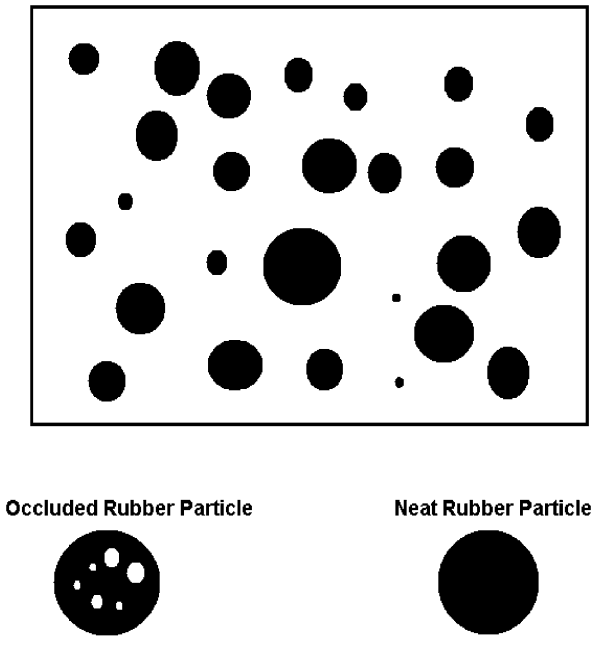

Fig. 1. Diagram of typical phase morphologies in rubber modified epoxy resins.

The objectives of this study are to: (1) use scanning electron microscopy (SEM) and atomic force microscopy (AFM) to determine the morphology and phase distribution of the rubber particles; (2) use AFM as a probe to measure the mechanical properties of the rubber particles.

2. Experimental

2.1. Materials

An epoxy resin, Epon 828 (Miller-Stephenson Chemical Co.), was modified with CTBN rubbers, Hycar 1300X31 and Hycar 1300X8 (B. F. Goodrich Chemical Corp.). The polymerization (cure) was initiated with piperidine used as the curing agent. The chemical formulas of the reactants are shown in Fig. 2. The phase morphology and rubber phase elastic modulus values were altered by varying the rubber acrylonitrile percentage, piperidine concentration, and cure temperature. Table 1 lists the compositions and cure temperatures for the rubber-modified epoxy samples that were prepared. The formulations are described in Table 2.

Piperidine is a cyclic secondary amine, which in reacting with an epoxy, first undergoes addition to the epoxy group via its labile hydrogen and then functions as a tertiary amine anionic initiator. The tertiary amine aduct also promotes the carboxyl-epoxy reaction.

The process used for preparation of the rubber-toughened epoxy samples [4,15] involves mixing CTBN rubber with the uncured epoxy resin. Note that in all of the formulations considered the rubber concentration is fixed at 15phr or

Table 1
Test matrix for rubber-toughened epoxy samples

Sample no.	Acrylonitrile percent	Piperidine concentration (phr)	Cure temperature (°C)
1	10	3	90
2	18	3	90
3	10	5	90
4	18	5	90
5	10	3	120
6	18	3	120
7	10	5	120
8	18	5	120
9	10	3	150
10	18	3	150
11	10	5	150
12	18	5	150

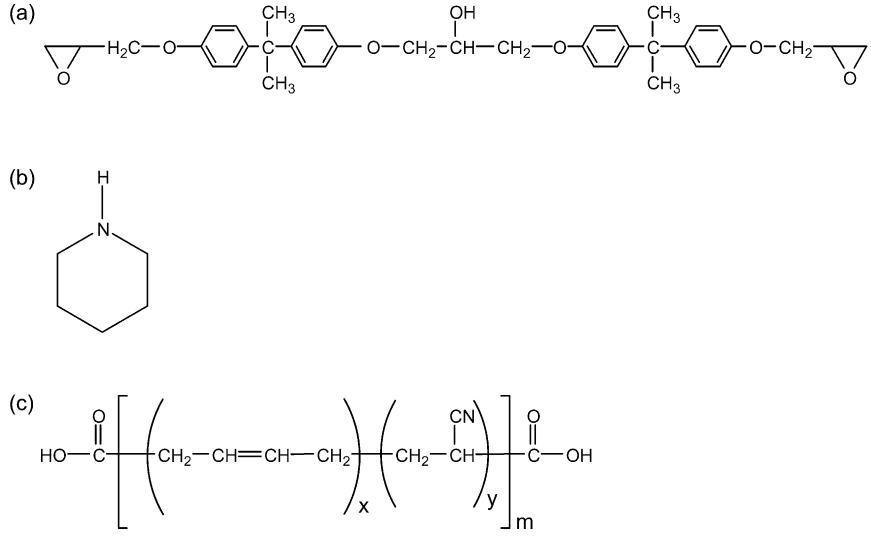

Fig. 2. Chemical structures of epoxy resin components for this study: (a) Epoxy oligomer, (b) Piperidine, (c) CTBN rubber.

12.5%(wt). The characterization data for the two CTBN rubbers are presented in Table 3. Typically, the two components are placed in a beaker and stirred by hand for 5–10 min. The mixture is then heated in a water bath to 60–70 °C and mixed with an electric stirrer for 5 min. It is next placed in a vacuum oven and degassed at 60 °C until frothing stops.

The mixture is then cooled to below 30 °C and piperidine is mixed in slowly to avoid entrapping air. Finally, the mixture is poured into a preheated mold and cured. The cure time is 16 h. After curing, the resulting polymer is cooled very slowly by allowing it to come to room temperature inside the oven [4,15].

2.2. Morphology studies

The phase morphology of the rubber-modified epoxy samples was evaluated using both SEM (Leo 440) and AFM (TA Instruments μTA 2990). Since both rubber particles and holes appear as similar features in AFM images, and surface roughness masks the phases of interest, it was necessary to prepare highly smooth samples. Such smooth sample surfaces were prepared by curing film samples on NaCl single crystals. A sodium chloride single crystal cube was broken along the crystal plane by tapping a razor blade parallel to a cube surface. By this method a single 10 mm cube can be broken into numerous smooth surfaces suitable for coating in order to prepare film specimens. The rubber and epoxy resin are mixed prior to polymerization and droplets are placed on a preheated sodium chloride crystal and allowed to level. The sample is then cured at the desired temperature. Finally, the sodium chloride is removed by dissolving with water. The film samples prepared by this method then were analyzed with both SEM and AFM.

2.2.1. Scanning electron microscopy (SEM)

In order to view phase separated CTBN rubber particles with SEM, the samples were stained with osmium tetroxide (OsO_4) [11,15]. The samples were placed for 15 min into a 1% OsO_4/tetrahydrofuran solution. The osmium reacts with the double bonds of the rubber to form a stable intermediate, which has a high electron capture crossection. When analyzed by SEM (secondary electron mode), the rubber particles appear as bright white spots.

2.2.2. Atomic force microscopy (AFM)

The smooth sample surfaces were also analyzed using contact mode AFM. This is a technique that generates an image by applying a force to a sharp mechanical probe and rastering it across the sample surface [19]. A laser beam is reflected off the back of the probe and focused onto a photodetector with a mirror. As the probe moves laterally in the *X*-direction, the laser beam strikes a different portion of the photodetector, thus generating a signal. The probe will penetrate deeper into the sample when scanning across a low modulus rubber particle than it will when going across

Table 2
Formulations of rubber-modified and unmodified epoxy samples (phr = parts per hundred by weight) [4]

Component	Unmodified epoxy (phr)	Rubber-modified epoxy (phr)
Epoxy resin	100	100
Piperidine	3 or 5	3 or 5
Carboxyl-terminated butadiene acrylonitrile rubber (CTBN)	NA	15

Table 3
CTBN characterization data

CTBN characteristic	1300×31	1300×8
Acrylonitrile (wt%)	10	18
Carboxyl content (acid number)	28	29
Molecular weight, M_n	3800	3500
DSC glass transition temperature (°C)	−66	−52

the high modulus epoxy matrix. This difference in penetration provides a means for characterizing localized differences in the stiffness or modulus of the sample.

In order to determine such changes in mechanical properties using AFM, the AFM probe's spring constant and contact area must be calibrated (see Appendix A for a description of probe calibration procedures). Once the rubber particles have been imaged by AFM, their elastic modulus at a given point can be determined through the use of force–distance curves (Fig. 3) [20–23]. The probe-tip is initially some distance away from the sample corresponding to point a on Fig. 3. The probe approaches the sample (corresponding to motion along line a–b from right to left) until the tip dips toward the sample surface (corresponding to point c). The tip deflection is due to an attractive force between the sample and probe. Such attractions arise due to several kinds of sample-probe tip interactions including capillary forces from adsorbed water and hydrocarbon contamination layers, electrostatic charges, or van der Waals forces [20].

The probe is then lowered causing it to deflect and indent into the surface until the predetermined force is reached (corresponding to movement from point c to point d). It is then removed from the sample (corresponding to movement from d to f). Because of the adhesion forces between the probe tip and the sample, the cantilever deflects downward until enough upward force is applied to lift the tip from the sample surface (corresponding to dashed line f–g). The slope of the unloading curve is the contact stiffness, S, which is related to the reduced elastic modulus, E^*, as indicated in Eq. (1) [22,23]:

$$S = \frac{\delta F}{\delta d_R} = \frac{2}{\pi} E^* A^{1/2} \tag{1}$$

where F is the force, d_R is the penetration distance, and A is the contact area. The reduced elastic modulus then can be used to calculate the modulus of the sample through the following expression [22,23]:

$$\frac{1}{E^*} = \frac{(1-\nu_s^2)}{E_s} + \frac{(1-\nu_p^2)}{E_p} \tag{2}$$

here ν_s is the Poisson's ratio of the sample, E_s is the elastic modulus of the sample, and ν_p and E_p are the Poisson's ratio and elastic modulus, respectively, of the probe.

2.2.3. Experimental plan and data analysis

A 2×2×3 matrix full factorial cure experiment was performed on the rubber-modified epoxy with the cure variables being piperidine concentration and cure temperature, along with weight percent of acrylonitrile in the rubber (see Table 1 for the test matrix). The study was replicated to provide statistically sound data. The data were analyzed using the SAS statistical data analysis software package (www.sas.com/technologies), to determine how the first-, second-, and third order cure condition interactions affect the rubber particle size, volume fraction, and modulus.

2.2.4. Dynamic mechanical analysis

The glass transition temperatures of cured samples were determined by dynamic mechanical analysis (DMA) with a

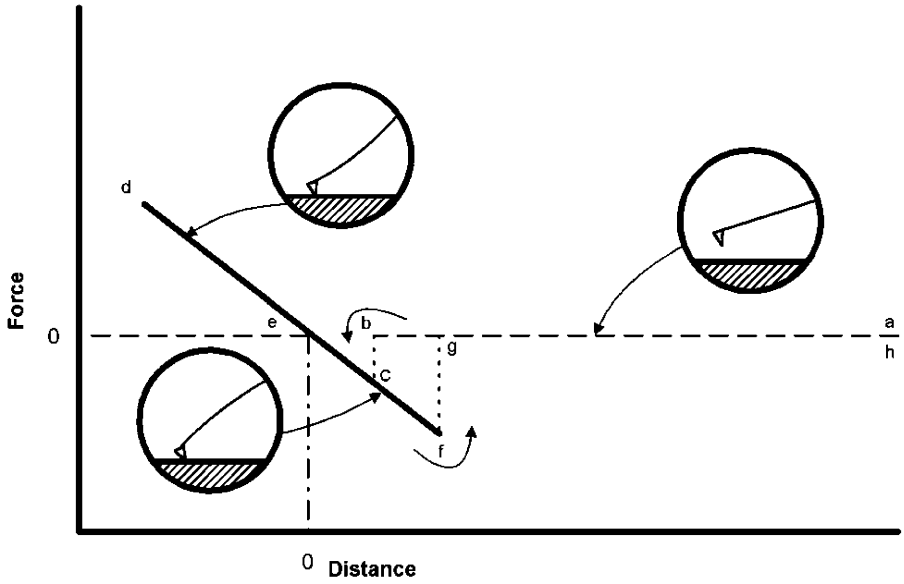

Fig. 3. An ideal force–distance curve for an infinitely hard surface [20].

TA Instruments DMA 2980 instrument. DMA is a well-known method for determining viscoelastic properties by applying a controlled sinusoidal strain to a sample and measuring the resulting stress. DMA gives both storage modulus and loss modulus characteristics as a function of temperature.

The DMA samples for this study were prepared in a silicone rubber mold and analyzed using a dual-cantilever test geometry. The DMA was operated at a frequency of 1 Hz using a temperature ramp of 2 °C/min, ranging from −100 to +150 °C. The rubber modified epoxy samples exhibit two T_gs, one at low temperatures for the rubber phase and one at a high temperature for the epoxy phase. The values recorded were taken at the peaks in the DMA loss modulus curve. In this paper the T_g value of primary interest is the low temperature rubber phase T_g.

2.2.5. Fracture toughness measurements

Standard compact tension specimens were used to determine the fracture toughness of the rubber modified epoxies. The specimens were prepared in a manner similar to the DMA specimens by curing in a silicone rubber mold. After cure they were secured in a fixture and a notch was cut by placing pressure on a razor blade and sliding the sample back and forth in a sawing motion. The depth of the notch was measured using an optical microscope. The samples were fractured in three-point bend mode at room temperature and at a strain rate of 1 mm/min. The stress was measured as a function of strain using a Rheometrics mini-materials tester (MiniMat 2000). The fracture toughness (K_Q) was calculated using the method of ASTM D 5045.

3. Results

3.1. Morphology

3.1.1. Scanning electron microscopy (SEM)

3.1.1.1. Rubber particle size. Inspection of the smooth samples by SEM showed that:

- There were no rubber particles on the surface of samples 1, 3, and 4.
- The sample morphology was highly dependent upon the rubber acrylonitrile % (Figs. 4 and 5).

The samples containing Hycar 1300X31 (10% acrylonitrile) had fewer but larger rubber particles (Fig. 4) than samples containing Hycar 1300×8 (18% acrylonitrile). As noted in the literature [9,15,24,25], CTBN rubbers that contain a greater percentage of acrylonitrile are more miscible with an epoxy resin and phase separate at a later stage in the polymerization. As vitrification is approached, the viscosity rises to a point where rubber diffusion becomes more limited. The results of SEM analysis of smooth surface samples are summarized in Table 4. There is a much wider range of particle sizes in samples containing Hycar 1300×31 (Table 4, odd sample numbers, and Fig. 4) than samples containing Hycar 1300×8 (Table 4, even sample numbers, and Fig. 5).

3.1.1.2. Rubber particle volume fraction. The rubber particle volume fraction was measured from SEM photomicrographs by image analysis equating the area fraction and volume fraction. It is interesting to note that even though phase separation occurs at a stage when rubber diffusion is more limited for samples containing Hycar 1300×8, the rubber particle volume fraction in these samples is noticeably larger than for samples containing Hycar 1300×31. This is due to a larger amount of epoxy resin dissolved and occluded in the phase separated rubber.

3.1.2. Atomic force microscopy (AFM)

3.1.2.1. Phase morphology. Since AFM is a surface analysis technique, only those rubber particles that transfix the sample surface are imaged (see Fig. 6 for a representative AFM image). Because it is unlikely that an entire imaged rubber particle is on the sample surface, rubber particle size and bulk composite morphological determinations by AFM may lead to misleading conclusions. Moreover, AFM imaging covers only a relatively small surface area, so it does not provide a representative analysis covering large numbers of the micrometer sized particles, even though we can study individual micron sized particles with AFM (Fig. 7 is a good example of this). AFM does, however, provide valuable information about nano-phase rubber particles. In Fig. 8, for example, some very small rubber particles are evident. Most of these are less than 40 nm in diameter. Though their exact size is not certain, the close proximity of one particle to another suggests that they are indeed quite small. These nano-dispersed particles are not seen in SEM images.

Until now SEM has been the primary method used for imaging the morphological features of rubber modified epoxies. AFM clearly adds additional details to our notion of phase separation in these systems. One might speculate that these nano-phase particles, not seen in SEM, represent a portion of the rubber that previously has been assumed to be dissolved in the epoxy phase rather than phase separated. In addition to the nano-dispersed rubber particles, an occluded epoxy phase that was not evident in SEM analysis was seen in some of the AFM images (Fig. 7). A more comprehensive study of the nano-phase rubber particles than that completed here would require the use of a very sharp probe. The AFM probe used in this study was blunt as discussed in the following paragraphs.

3.1.2.2. Rubber phase modulus. A single AFM probe was used in the morphology and rubber particle modulus determination. The probe calibration procedure and results

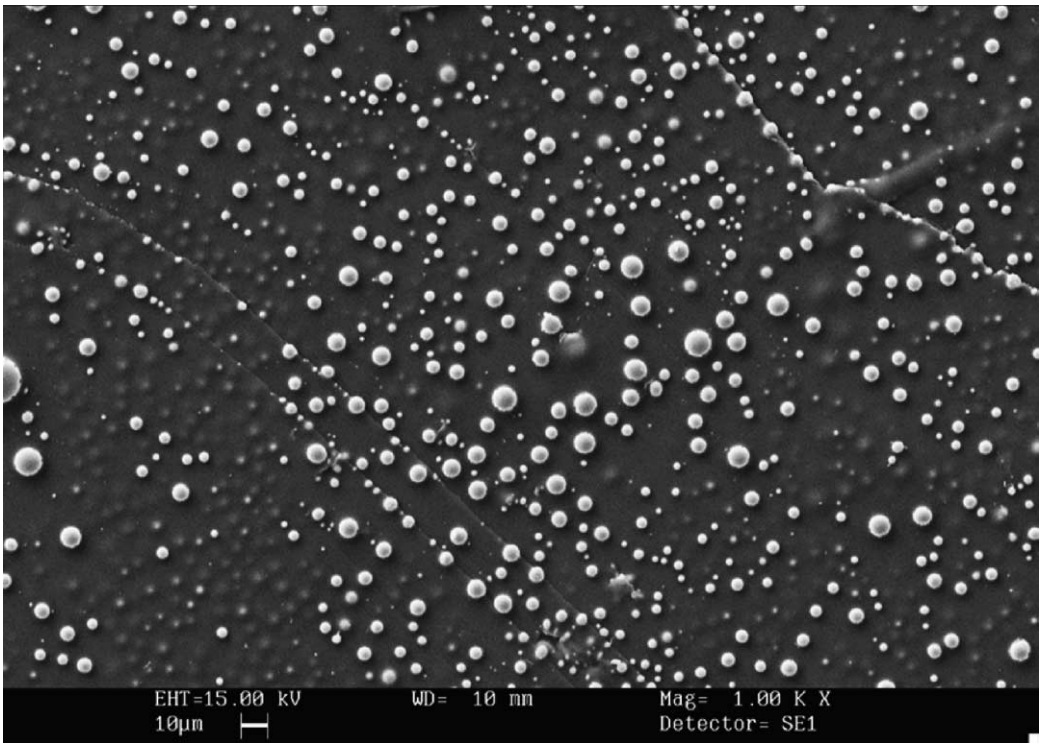

Fig. 4. SEM image (1000× magnification) showing the morphology of sample 5 (see Table 1 for composition and cure temperature).

as referred to previously, are discussed in Appendix A. The contact area calibration (Appendix A) indicated that the modulus was very sensitive to small changes in the contact area. Such small changes in the contact area could not be determined with complete certainty, so that the AFM elastic modulus values reported may be slightly inaccurate.

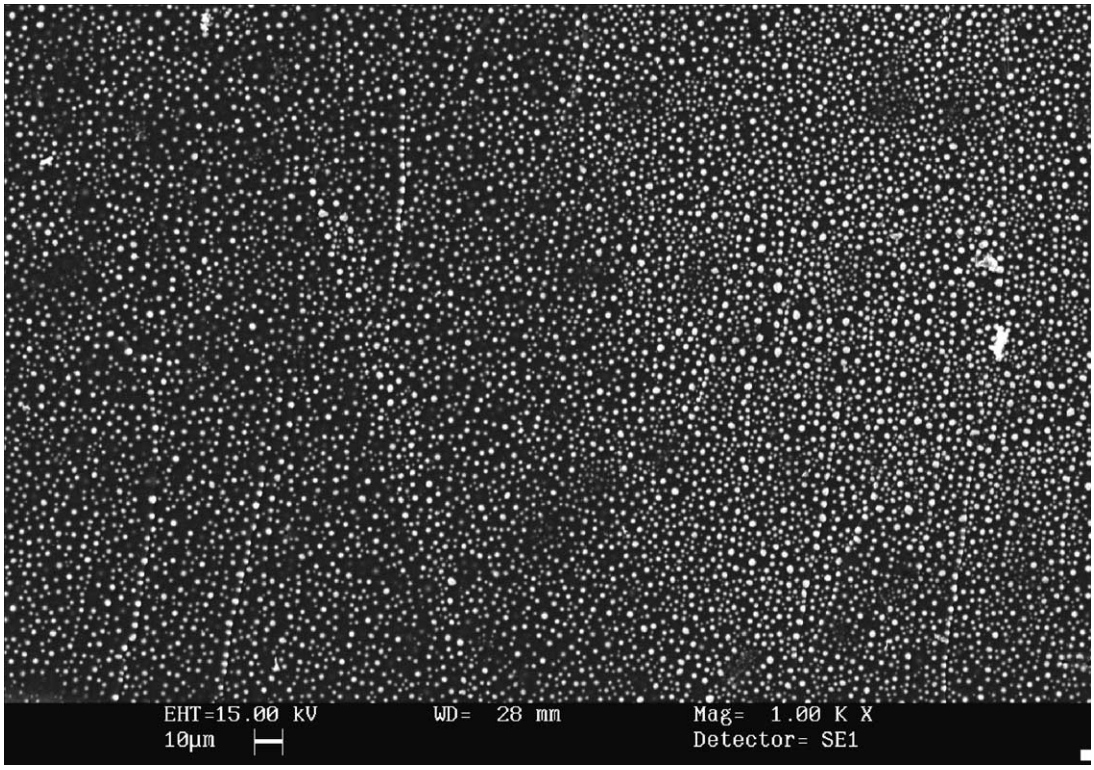

Fig. 5. SEM image (1000× magnification) showing the morphology of sample 6 (see Table 1 for composition and cure temperature).

Table 4
Rubber particle sizes and volume fractions for osmium stained smooth samples

Sample no.	2	5	6	7	8	9	10	11	12
Mean particle diameter (μm)	1.098	2.979	1.251	3.704	1.074	6.695	1.178	3.873	1.138
Standard deviation	0.377	1.555	0.423	2.454	0.356	2.772	0.602	1.867	0.420
Rubber volume fraction	0.159	0.087	0.150	0.083	0.170	0.131	0.243	0.182	0.219
Number of particles counted	248	787	188	451	286	265	303	1012	318
Scan area (μm^2)	50×40	380×240	50×40	380×240	50×40	380×240	50×40	380×240	50×40

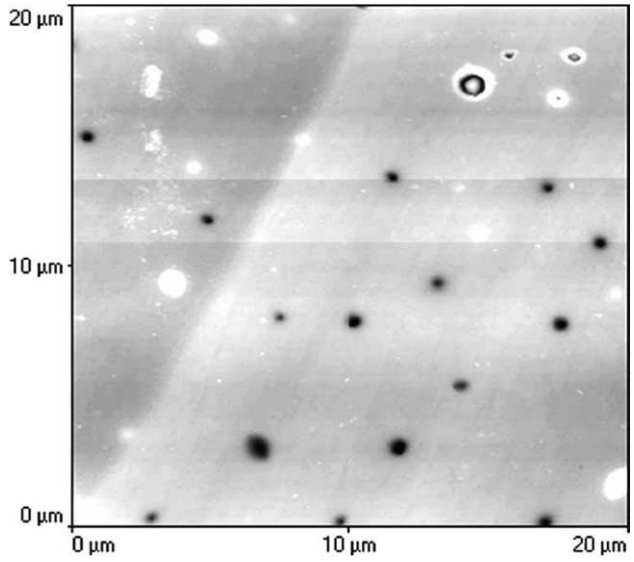

Fig. 6. AFM contact-mode image of sample 6 (see Table 1 for composition and cure temperature) showing the dispersed rubber phase (black spheres) and a smooth sample surface.

However, the degree of uncertainty in all of the values is the same so that the values are certainly precise. The contact area used for the modulus determinations was calculated using a crosslinked CTBN sample.

All of the force–distance curves in this study were linear (see Appendix B for the method used to convert arbitrary force–distance curves to absolute force–distance curves). This result deviated from the work of Doerner and Nix [21], Oliver and Pharr [22], and VanLandingham et al. [23] who showed curves that were not linear. Doerner and Nix [21], however, argued that a portion of their force–distance curves were linear. Two reasons that the force distance curves are linear in this study are: (1) much smaller forces were applied to the samples in this study (<80 nN vs. $>$ 500 nN [21]); and (2) the probe tip was flat as indicated in the SEM image of the probe tip (Fig. 9). When very small stresses are applied to a sample, plastic deformation does not occur. There was little difference in five separate force–distance curve determinations taken at a single point indicating that no permanent plastic deformation occurred. The forces applied are still in the linear, recoverable portion of the stress strain curve. This accounts for the linear force–distance curve. In addition, according to the literature [22,23,26], force distance curves determined using a flat 'cylindrical punch' should be linear.

Since the scope of this study was to evaluate the elastic modulus of very small rubber particles, small forces are required in order to limit the volume of material involved in the deformation. Large forces would not only deform the rubber particles, but also the epoxy matrix, leading to erroneous elastic modulus determinations. Table 5 summarizes the rubber particle modulus data. In each case the number of particles analyzed was limited to the number of particles that were visible on a sample surface.

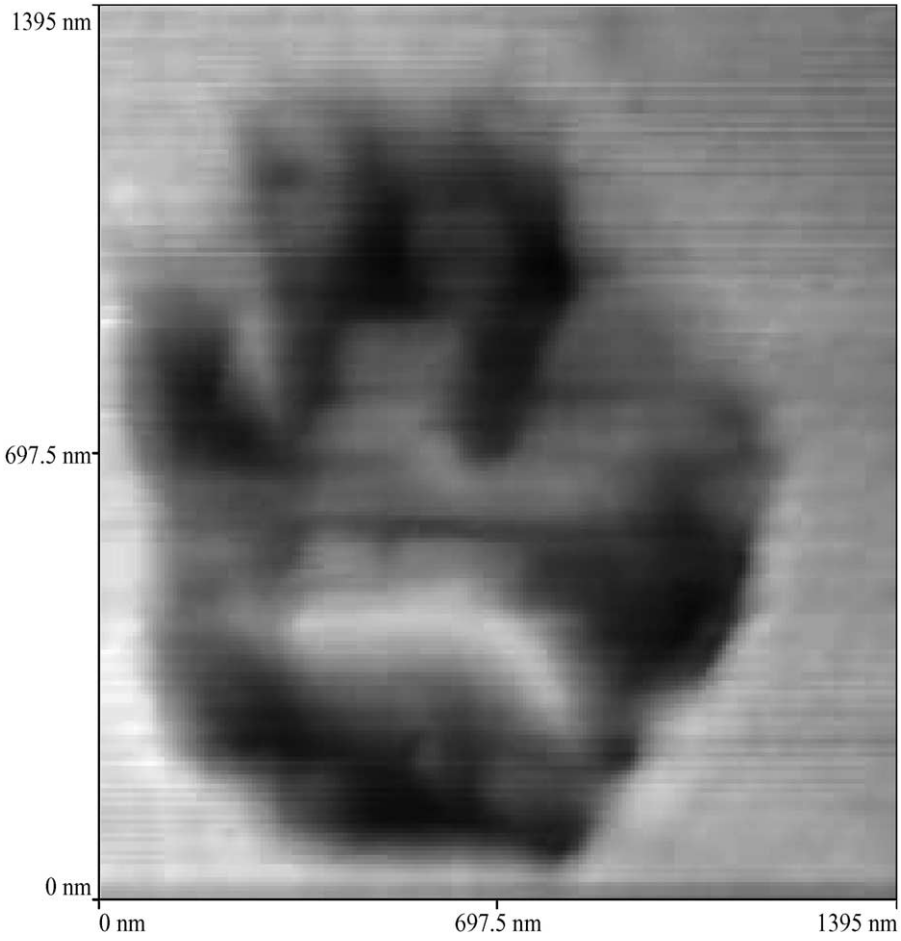

Fig. 7. AFM scan of a single rubber particle in sample 5 showing the occluded epoxy phase in the rubber particle; particle size is ~1 μm (refer to Tables 1 and 2 for composition and cure temperature).

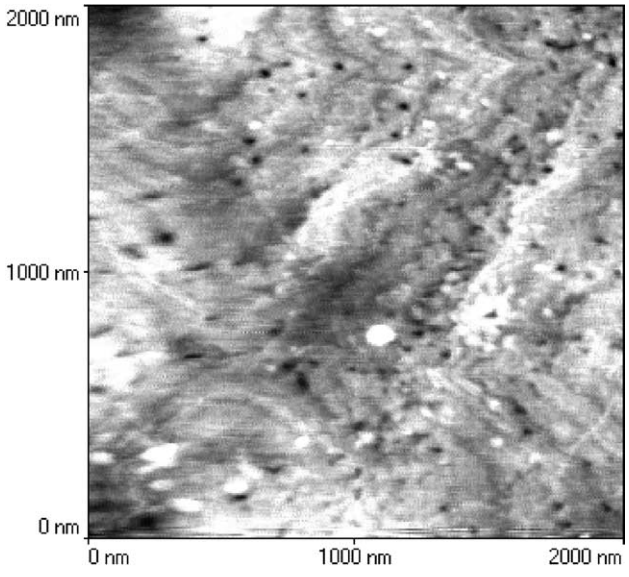

Fig. 8. 2000 nm scan of sample 6 (see Table 1 for composition and cure temperature) showing the presence of nano-phase rubber particles.

4. Discussion

The data were evaluated statistically using the SAS statistical analysis software, to determine how the cure variables i.e. rubber acrylonitrile %, piperidine concentration, and cure temperature affect the mean rubber particle size, rubber particle volume fraction, and rubber particle modulus. An analysis of variance (ANOVA) was performed to determine only the principal effects. Variables that exhibited a very strong effect (probability <0.01), strong

Table 5
AFM elastic modulus values for rubber particles

Sample no.	Mean particle modulus (MPa)	Standard deviation	Number of particles analyzed
2	7.16	0.00004	4
5	7.29	0.00007	6
6	6.79	0.00017	7
7	7.28	0.00005	5
8	7.21	0.00000	2
9	6.49	0.00033	3
10	6.39	0.00002	3
11	6.27	0.00007	7
12	6.20	0.00005	2

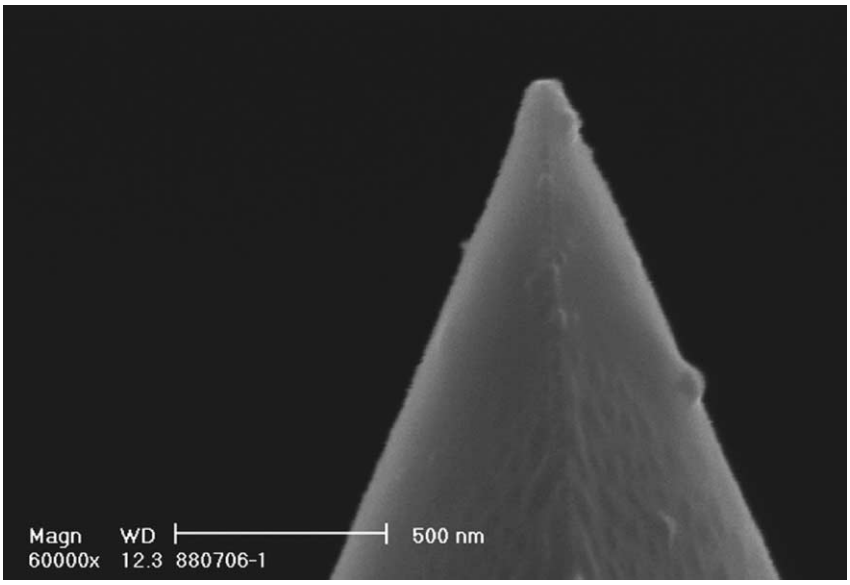

Fig. 9. High Magnification SEM image of the AFM probe tip used in this study.

effect (probability between 0.01 and 0.05) or moderate effect (probability between 0.05 and 0.10) were reanalyzed using a means statement. Only the data for samples cured at 120 and 150 °C were evaluated statistically because no rubber particles were observed on the surface of three of the samples cured at 90 °C (samples 1, 3, and 4).

4.1. Rubber particle size

The ANOVA indicated that the rubber acrylonitrile % has a strong effect on the rubber particle size. The means statement indicates that the largest rubber particles occur when rubber with 10% acrylonitrile is added (Table 1—odd numbered specimens). As discussed in Section 3.1, this is to be expected because the 10% acrylonitrile rubber is less soluble in the epoxy than the 18% acrylonitrile rubber. Thus, in this case the rubber phase separates earlier in the polymerization [9,15,24,25]. Early in the cure the viscosity is relatively low so rubber can diffuse more readily to form large particles.

4.2. Rubber particle volume fraction

The ANOVA also suggested that the rubber acrylonitrile % as well as the cure temperature strongly affect the rubber particle volume fraction. The means statement indicates that the highest rubber particle volume fraction occurs with 18% acrylonitrile (see Table 4- even sample numbers) and the 150 °C cure temperature (see Table 4, samples 9–12). Since both of these variables favor increased miscibility [24], the rubber particle volume fraction that results is greater than the actual volume of the rubber. This is due to an increase in the amount of epoxy resin occluded within the rubber particles.

4.3. Rubber phase modulus

For each of the samples, the glass transition for the rubber phase was clearly evident from the dynamic mechanical loss modulus peak. As noted in Table 6, the T_gs for the rubber phase in the rubber modified samples are higher than those of the bulk rubber. This is consistent with the fact that there is some epoxy dissolved and/or occluded in the rubber phase. The T_g values are expected to be directly related to the amount of epoxy in the rubber phase. By applying the Fox equation [27] to the glass transition data, the weight fraction of rubber in the rubber phase was estimated to range from 0.77 to 0.94. The T_g data of Fig. 10 show an almost linear relationship with composition, consistent with the Fox equation. However, there is no

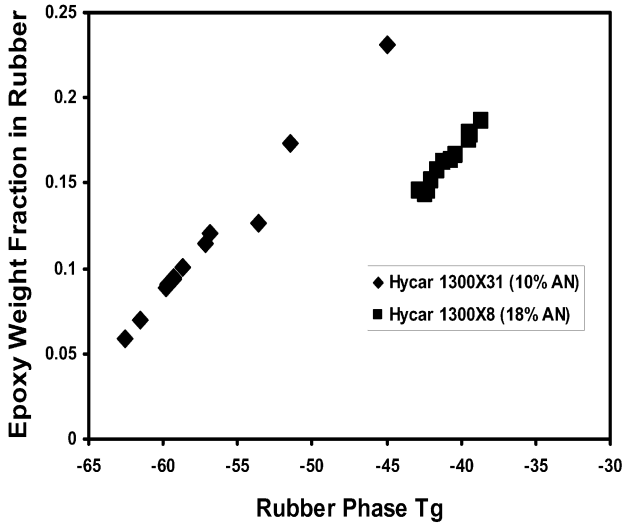

Fig. 10. Relation between rubber phase T_g values and epoxy content of the rubber phase. The bulk rubber T_g values are, respectively, −68 and −56 °C.

Table 6
Glass transition temperatures for the rubber phase

Sample no.	Number of measurements	Mean T_g (°C)	Standard deviation	Bulk rubber T_g (°C)
1	2	−55.3	2.26	−68.1
2	2	−40.4	1.22	−56.1
3	2	−52.1	10.16	−68.1
4	2	−39.9	0.63	−56.1
5	2	−55.1	5.06	−68.1
6	2	−42.2	0.89	−56.1
7	2	−59.8	3.85	−68.1
8	2	−42.4	0.07	−56.1
9	2	−59.5	0.23	−68.1
10	2	−39.0	0.52	−56.1
11	2	−59.9	1.27	−68.1
12	2	−41.4	0.92	−56.1

apparent relationship between the rubber particle modulus and rubber phase T_g, as indicated in Table 6.

According to the statistical analysis, the ANOVA indicated that the cure temperature has a dominant effect on the rubber particle modulus. The means statement indicates that the highest rubber particle modulus occurs at the 120 °C cure temperature (see Table 5, samples 5–8).

This result is unexpected, since the rubber particle modulus generally is thought to be related to the dissolved epoxy resin concentration in the dispersed rubber phase [28]. An increase in dissolved epoxy resin is expected to result in an increase in the rubber particle modulus. The morphology data in Table 4 indicate that a larger volume of epoxy is occluded in the rubber of samples cured at 150 °C. However, the rubber particle moduli of samples cured at 150 °C are lower than those of samples cured at 120 °C. Thus the data suggest that the rubber particle modulus may be more dependent upon the strain induced in the rubber particles as a result of matrix curing rather than on the occluded epoxy resin content. As the rubber particles are stretched into a more constrained conformation, chain stiffening occurs. Since the elastic modulus is related to stiffness, a highly constrained rubber particle will have a higher modulus than a less constrained rubber particle.

The strain is the result of at least three factors. These are: (1) the cure shrinkage of the matrix surrounding the particles; (2) the rigidity or modulus of the matrix after cure prior to cooling; and (3) the differential in coefficient of thermal expansion (CTE) between the rubber particles and the epoxy matrix near the particle interface during cooling. Certainly the rubber phase has a larger CTE than the epoxy phase [4–6,8,9,29]. We determined that the T_gs of the epoxy phase for samples cured at 120 °C are in the range of 93–95 °C, for the 150 °C samples epoxy phase T_gs are in the range of 86–88 °C. So the effective temperature range where the CTE mismatch is important during cooling is greater for the 120 °C samples. The effect of matrix cure shrinkage and matrix modulus on the rubber phase may be interpreted as follows. The samples cured at 150 °C have a lower modulus at the cure temperature. At 150 °C the samples are actually in the (viscoelastic) plateau region after cure (but before cooling). Thus cure strains transferred to the particles due to shrinkage of the matrix have an opportunity to fully relax before the sample is cooled. On the other hand, samples cured at 120 °C are in the transition region where the matrix is much more rigid. In this case the stresses transferred due to matrix cure shrinkage may not have an opportunity to relax prior to cooling.

A further note here by way of explanation, the lower epoxy phase T_g values for the samples cured at 150 °C may arise due to evaporation of some of the piperidine during the cure cycle. Piperidine has a boiling point of 109 °C. Such an effective reduction of the piperidine content would lead to a lower crosslink density and therefore, a lower T_g in the affected samples.

4.4. Relating morphology to fracture toughness

It is known that the morphology of the cured system, particularly the particle size and volume fraction of the rubber phase, affect the degree to which the epoxy is toughened. The volume fraction is considered to be the key factor [6,7,9,13,14,16,18]. As the particle volume fraction increases toughness increases, so that the two-phase occluded particle morphology is preferred. It is not well known, however, how the specific mechanical properties of the rubber phase affect the toughness.

In Fig. 11 we see that, indeed, the toughness is found to

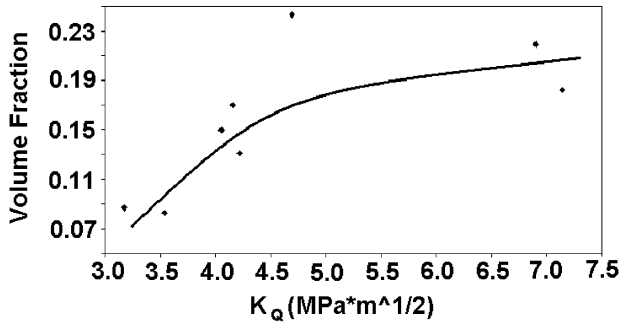

Fig. 11. Variation in fracture toughness with volume fraction of rubber phase.

increase with volume fraction. However, the data of Fig. 12 indicate that the toughness is greatest when the particle modulus values do not exceed ~6.2 MPa. So it appears that, while a larger volume fraction of rubber usually favors enhanced toughness, increased volume fraction by itself may not always result in increased toughness. The particles also must be sufficiently 'soft' in order to improve toughness. In the system of interest here, the processing conditions are a key factor in achieving the most appropriate material properties.

5. Conclusions

Scanning electron microscopy (SEM) and atomic force microscopy (AFM) were used to determine the morphology and phase distribution of the dispersed rubber particles in a rubber-modified epoxy resin. By SEM it was verified that different rubber acrylonitrile contents (%) resulted in different morphologies. This is consistent with expected trends. In general the rubber particle populations observed with SEM were in the 1 10 μm range. Epoxy resin samples modified with CTBN rubber having a low acrylonitrile % have much larger rubber particles and a broader particle size distribution than epoxy samples modified with CTBN rubber that has a higher acrylonitrile %.

AFM only detects the rubber particles that reside at and penetrate through the sample surface and is not suitable for bulk morphology determinations. It does, however, have the potential for providing information concerning the presence of nano-phase dispersed rubber particles. Particles <40 nm in size were noted in AFM images. These nano-dispersed rubber particles were not found in the SEM images. It is speculated that the portion of the rubber represented by these particles has been assumed by previous researchers to be dissolved in the epoxy phase rather than phase separated. With the proper scanning conditions, specifically a very sharp probe, AFM is a technique capable of studying this nano-dispersed phase in more detail.

Occluded epoxy phase was found in some of the micrometer sized rubber particles with AFM but was not observed with SEM. In addition, an AFM probe was calibrated and quantitative rubber particle modulus values were measured using force–distance curves. It was shown that by generating force–distance curves using a flat probe tip and by applying very small forces, linear curves are obtained.

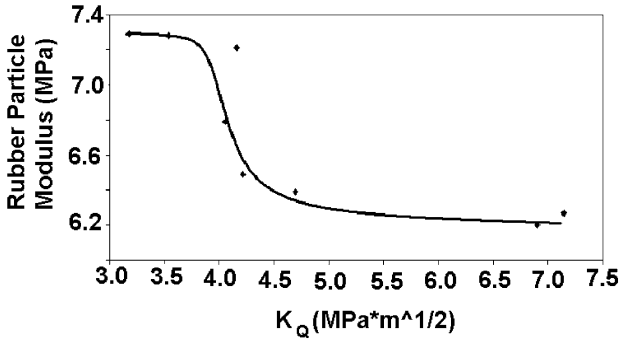

Fig. 12. Relation of resin fracture toughness to modulus of rubber phase.

Prior to this research, it was assumed that as the amount of epoxy resin occluded in the rubber phase increased, the rubber particle modulus also would increase. However, the data presented here indicate a different effect. The rubber particle modulus instead appears to be more closely related to the amount of constraint on the rubber particles.

Statistical analysis of the morphology data showed that the rubber acrylonitrile % had an effect on both the rubber particle size and volume fraction. The largest particles resulted in samples with rubber containing 10% acrylonitrile (mean rubber particle size = 4.31 μm). The largest rubber particle volume fraction was in the samples containing rubber with 18% acrylonitrile (mean volume fraction = 0.19). The cure temperature had an effect on the rubber particle volume and modulus. The volume fraction of rubber phase was largest at a cure temperature of 150 °C (mean volume fraction = 0.19) and the rubber particle modulus was highest at a cure temperature of 120 °C (mean modulus = 7.14 MPa).

Consistent with conventional wisdom about morphology-property relationships in these systems, rubber particle volume fraction was found to be a key factor. However, the data of this study indicate that the toughness is greatest when the particle modulus values do not exceed ~6.2 MPa. So it appears that, while a larger volume fraction of rubber usually favors enhanced toughness, increased volume fraction by itself may not always result in increased toughness. The particles also must be sufficiently 'soft' in order to improve toughness. In the system of interest here, the processing conditions are a key factor in achieving the most appropriate material properties.

Appendix A. Calibration of AFM cantilever

A.1. Spring constant calibration

The force applied to a polymer sample is a function of the probes spring constant. Probe's can be purchased with a broad range of spring constants. The spring constant is a function of the material used to make the probe and the probe's dimensions. There are many methods for determining spring constants [30–37]. Two simple methods for determining the spring constant of an AFM cantilever are: (1) beam theory [20,30,31,34]. (2) The use of a calibration cantilever [36,37].

A.1.1. Beam theory

According to beam theory, the spring constant is a function of the probes dimensions and the elastic modulus of the probe's material (typically silicon). The spring constant, k, is calculated as [20,30,31,34]:

$$k = \frac{Et^3 w}{4l^3} \tag{A1}$$

where E is the elastic modulus of the material used to make the probe, t is the thickness of the cantilever, w is the width of the cantilever, and l is the distance from the probe's base to the probe tip.

In this study, the dimensions were determined by scanning electron microscopy (SEM). Table 7 summarizes the dimensions and calculated spring constant using beam theory.

A.1.2. Calibration cantilever

The calibrated cantilever used in this study (purchased from Veeco Metrology group) has a spring constant, k_{ref}, of 0.283 N/m. Calibration of the probe's spring constant using this method [36,37] involves measuring the slope the cantilever makes with the sample surface, θ ($\sim 10^\circ$), and determining the force–distance curve slopes of sapphire (infinitely hard surface), δ_{tot}, and the calibration cantilever, δ_{ref}. The spring constant is then calculated as [36,37]:

$$k_{test} = k_{ref} \frac{\delta_{tot} - \delta_{ref}}{\delta_{ref} \cos\theta} \tag{A2}$$

In this study, five measurements of slope were averaged as:

$\delta_{tot} = 0.1041$ nA/nm

$d_{ref} = 0.0774$ nA/nm

The calculated probe spring constant, k_{test}, is 0.099 N/m. The values of probe spring constant calculated using Beam Theory [22,32,33,36] (0.109 N/m) and a calibrated cantilever [36,37] (0.099 N/m) agree very well. In the calculation of elastic modulus of the rubber particles, the calibrated cantilever method value is used because it accounts for variations in the probe's dimensions.

A.2. Contact area calibration

The probe's contact area was calculated at multiple temperatures for rigid poly(vinyl chloride), polycarbonate, poly(ethylene terephthalate), high density polyethylene, low density polyethylene, cured epoxy resin, and vulcanized CTBN rubber. Multiple materials were selected to determine if the contact area for one material is applicable to other materials and multiple temperatures were selected to determine if the contact area remained constant as the material changed upon heating. The contact area, A, is calculated as [22,23]:

Table 7
Probe dimensions and beam theory spring constant

Width (w)	48.75 μm
Length (l)	414 μm
Thickness (t)	1.52 μm
Spring constant	0.109 N/m

$$A^{1/2} = \left(\frac{\delta F}{\delta d_R}\right)\left(\frac{\pi^{1/2}}{2E^*}\right) \tag{A3}$$

where $\frac{\delta F}{\delta d_R}$ is the slope of the force–distance curve. The samples were heated on a temperature stage. A thermocouple was mounted to the sample surface since a variation in temperature of the sample stage and sample surface is to be expected due to thermal conductivity.

The reduced elastic modulus, E^*, can be calculated as [22,23]:

$$\frac{1}{E^*} = \frac{(1-\nu_s^2)}{E_s} + \frac{(1-\nu_p^2)}{E_p} \tag{A4}$$

where ν_s and ν_p are the Poisson's ratio for the sample and the probe and E_s and E_p are the storage modulus of the sample and probe. The storage modulus was determined using dynamic mechanical analysis.

The square root of the contact area was plotted as a function of storage modulus (Fig. A1). This plot shows that a very small change in contact area results in drastically different values of storage modulus for samples between 0.25 and 4.0 GPa. For example the difference in the square root contact area at 4 and 2 GPa is only 0.02455 nm. Below 0.25 GPa, the contact area increases rapidly as modulus decreases. Since the contact area is calculated from the slope of the force–distance curve, very small changes in the slope result in large changes in the storage modulus determinations. However, the effects of heating of the probe were not considered in these measurements. As the probe is heated, the probes' dimensions could change resulting in changes in the probes' spring constant. In addition, the contact area could change. Thus, the changes in the contact area versus storage modulus plot (Fig. A1) could be due to the heating of the probe.

Before the AFM can accurately determine the modulus of a polymer, a better method for determining contact area must be developed. The square root contact area (4.52 nm) used for the modulus determinations of phase separated rubber was calculated from a CTBN sample that was crosslinked with 4,4′-methylenedianiline.

Appendix B. Conversion of force–distance curves from arbitrary values to absolute values

Both the force and the distance are dependent upon the probe's spring constant. Therefore the force distance curves must be converted from arbitrary to absolute force–distance curves in a graphing program such as Microsoft Excel. The microTA 2990 software records the vertical axis of the force–distance curve in nano-amps (nA) and the horizontal axis in scanner motion distance, d (probe deflection plus sample penetration depth). To convert force from nA to nano-newtons (nN), a conversion factor, K (nA/nN), is calculated as [20]:

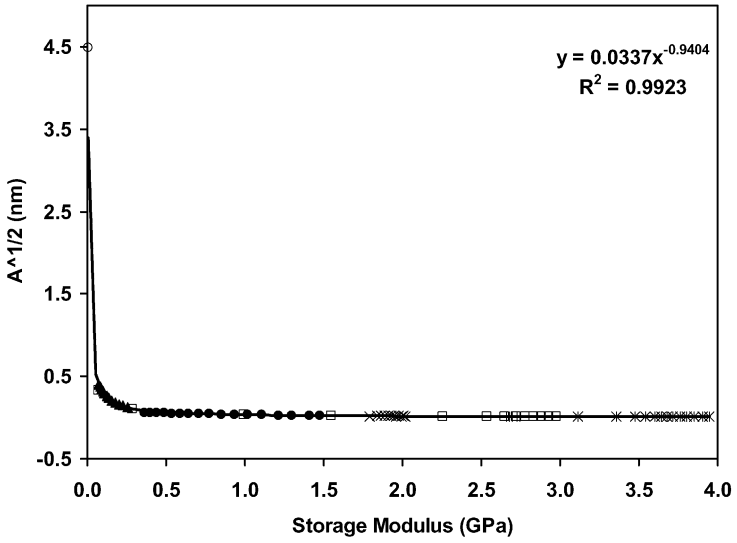

Fig. A1. Power law plot of the calculated contact areas versus storage modulus for rigid poly(vinyl chloride) (□), poly(ethylene terephthalate) (▲), polycarbonate (×), low density polyethylene (✳), high density polyethylene (♦), epoxy resin (+), and vulcanized CTBN (○).

$$K = \frac{k}{\delta_{\text{tot}}} \tag{B1}$$

where k is the probe's spring constant (see Appendix A) and δ_{tot} is the slope of a sapphire (infinitely hard surface) force–distance curve. This conversion factor is then multiplied by the force values to convert them from nA to nN. The penetration depth, d_{R}, at each point is calculated as [20]:

$$d_{\text{R}} = d - \frac{F}{\delta_{\text{tot}}} \tag{B2}$$

where F is the force at that specific point. Once these data are converted, a true force–distance curve can be plotted.

References

[1] Odian G. Principles of polymerization. 3rd ed. New York: Wiley; 1991 p. 109.
[2] Fried JR. Polymer science and technology. vol. 4 1995 p. 255–256, 272–275, 327–330.
[3] McGarry, FJ. Rubber in crosslinked glassy polymers (paper no. 86 delivered at the 129th meeting of the ACS Rubber Division, New York City, 8–11 April 1986), 1–9.
[4] Kinloch AJ, et al. Deformation and fracture behavior of a rubber-toughened epoxy: 1. Microstructure and fracture studies. Polymer 1983;24:1341–54.
[5] Huang Y, et al. Mechanisms of toughening thermoset resins. In: Riew CK, Kinloch AJ, editors. Toughened plastics I. Washington DC: American Chemical Society; 1993 [Chapter 1].
[6] Chan LC, et al. Rubber modified expoxies: cure transitions, and morphology. In: Riew CK, editor. ACS advancements in chemistry series 208. Washington DC: American Chemical Society; 1984.
[7] Cho, J. Rubber toughening of bismaleimide composite matrix resin. Ph.D. diss., University of Dayton. 91; 1990 107–109.
[8] Ratna D. Phase separation in liquid rubber modified epoxy mixture. Relationship between curing conditions, morphology and ultimate behaviour. Polymer 2001;42:4209–18.
[9] Hwang J-F, et al. Structure-property relationships in rubber-toughened epoxies. Polym Eng Sci 1989;29:1466–76.
[10] Sultan JN, McGarry FJ. Effect of rubber particle size on deformation mechanisms in glassy epoxy. Polym Eng Sci 1973;13:29–34 [no. 1].
[11] Bucknall CB, Yoshii T. Relationship between structure and mechanical properties in rubber-toughened epoxy resins. Br Polym J 1978;10:53–9.
[12] Azimi HR, Pearson RA, Hertzberg RW. Fatigue of rubber-modified epoxies: effect of particle size and volume fraction. J Mater Sci 1996; 31:3777–89.
[13] Kunz SC, Beaumont PWR. Low temperature behaviour of epoxy-rubber particulate composites. J Mater Sci 1981;16:3141–52.
[14] Guild FJ, Kinloch AJ. Modelling the properties of rubber-modified epoxy polymers. J Mater Sci 1995;30:1689–97.
[15] Manzione LT, Gillham JK, McPherson CA. Rubber-modified epoxies. I. Transitions and morphology. J Appl Polym Sci 1981;26:889–905.
[16] Kinloch AJ, Young RJ. Toughened multiphase plastics. In: Fracture behavior of polymers. New York: Applied Science Publishers; 1983. p. x p. 422 [chapter 11].
[17] Kinloch AJ, et al. Deformation and fracture behavior of a rubber - toughened epoxy: 1. Microstructure and fracture studies. Polymer 1983;24:1355–63.
[18] Huang Y, Kinloch AJ. Modelling the toughening mechanisms in rubber-modified epoxy polymers part I: finite element analysis studies. J Mater Sci 1992;27:2753–62.
[19] Price D. Thermal methods and atomic force microscopy: introducing these new friends (paper presented at the second international micro-TA symposium, Bowling Green, KY, May 8–9) 2000 p. 16–39.
[20] Mareanukroh, M., Use of atomic force microscope as a nanoindenter to characterize elastomers, (Ph. D. Diss., University of Akron, May 1999).
[21] Doerner MF, Nix WD. A method for interpreting the data from depth-sensing indentation instruments. J Mater Res 1986;4:601–9.
[22] Oliver WC, Pharr GM. An improved technique for determining hardness and elastic modulus using load and displacement sensing indentation experiments. J Mater Res 1992;7:1564–83.
[23] VanLandingham MR, et al. Nanoindentation of polymers: an overview. Macromol Symp 2001;167:15–43.
[24] Manzione LT, Gillham JK, McPherson CA. Rubber-modified epoxies. II. Morphology and mechanical properties. J Appl Polym Sci 1981;26: 907–19.

[25] Wise CW, Cook WD, Goodwin AA. CTBN rubber phase precipitation in model epoxy resins. Polymer 2000;41:4625–33.
[26] VanLandingham MR, et al. Nanoscale indentation of polymer systems using atomic force microscope. J Adhesion 1997;40:31–59.
[27] Fox TG. Bull Am Phys Soc 1956;1:123.
[28] Kunz-Douglass S, Beaumont PWR, Ashby MF. A model for the toughness of epoxy-rubber particulate composites. J Mater Sci 1980; 15:1109–23.
[29] Guild FJ, Young RJ. A predictive model for particulate filled composite materials part 2: soft particles. J Mater Sci 1989;24: 2454–60.
[30] Holbery JD, et al. Experimental determination of scanning probe microscope cantilever spring constants using a nanoindentation apparatus. Rev Sci Instrum 2000;71:3769–76.
[31] Gibson CT, Watson GS, Mybra S. Determination of the spring constants of probes for force microscopy/spectroscopy. Nanotechnology 1996;7:259–62.
[32] Smith ST, Howard LP. A precision low-force balance and its application to atomic force microscope probe calibration. Rev Sci Instrum 1994;4:903–9.
[33] Sader JE, Chon JWM, Mulvaney P. Calibration of rectangular atomic force microscope cantilevers. Rev Sci Instrum 1999;70:3967–9.
[34] Cleveland JP, et al. A nondestructive method for determining the spring constant of cantilevers for scanning probe microscopy. Rev Sci Instrum 1993;64:403–5.
[35] Sader JE, et al. Method for the calibration of atomic force microscope cantilevers. Rev Sci Instrum 1995;66:3789–98.
[36] Torii A, et al. A method for determining the spring constant of cantilevers for atomic force microscopy. Measurement Science Technology 1996;7:179–84.
[37] Tortonese M, Kirk M. Characterization of application specific probes for SPMs. Micromachining and imaging SPIE proceedings reprint. vol. 3009: Society of photo-optical instrumentation engineers; 1997 p. 53–60.